Electronic Supplementary Material (ESI) for Catalysis Science & Technology.

Tuning CO_2 hydrogenation selectivity on Ni/TiO_2 catalysts via sulfur addition

C. Le Berre, A. Falqui, A. Casu, T. T. Debela, M. Barreau, C. H. Hendon, P. Serp

SUPPORTING INFORMATIONS

Figure S1. The curves of: **a** CO_2 conversion; and **b** STY and c selectivity *versus* ToS at different temperatures over the $10Ni/TiO_2$ catalyst; reaction conditions: 200 mg catalyst, *F/W* = 33 000 $mL.g^{-1}.h^{-1}$, H_2/CO_2 = 4, 6.1 bar.

Figure S2. The curves of the CO_2 conversion and selectivity *versus* ToS at different temperatures over the $10Ni/TiO_2$ (black squares) and $10Ni\text{-}S/TiO_{2\text{-}rutile}$ (red circles) catalysts; reaction conditions: 200 mg catalyst, *F/W* = 16 500 $mL.g^{-1}.h^{-1}$, H_2/CO_2 = 4, 6.1 bar.

Table S1. Catalytic performances of supported Ni-based catalysts for the RWGSR.

Figure S3. The curves of the CO_2 conversion, conversion rate and selectivity *versus* ToS at different *F/W* ratio over the $10Ni\text{-}S/TiO_2$ catalysts. **a** CO_2 conversion at *F/W* = 16 500 $mL.g^{-1}.h^{-1}$ (red circles) and *F/W* = 33 000 $mL.g^{-1}.h^{-1}$ (black circles); and CO_2 conversion rate at *F/W* = 16 500 $mL.g^{-1}.h^{-1}$ (red squares) and *F/W* = 33 000 $mL.g^{-1}.h^{-1}$ (black squares). **b** Selectivity towards CO at *F/W* = 16 500 $mL.g^{-1}.h^{-1}$ (red diamonds) and *F/W* = 33 000 $mL.g^{-1}.h^{-1}$ (black diamonds).

Figure S4. The curves of the CO_2 conversion, conversion rate and selectivity *versus* ToS at different pressure over the $10Ni\text{-}S/TiO_2$ catalysts. **a** CO_2 conversion at 6.1 bar (red circles) and 1 bar (black circles); and CO_2 conversion rate at 6.1 bar (red squares) and 1 bar (black squares). **b** Selectivity towards CO at 6.1 bar (red diamonds) and 1 bar (black diamonds).

Figure S5. The curves of the CO_2 conversion and CO selectivity *versus* ToS at different temperatures over the $1Pt/TiO_2$ (black circles) and $10Ni\text{-}S/TiO_2$ (red circles) catalysts; reaction conditions: 200 mg catalyst, *F/W* = 16 500 $mL.g^{-1}.h^{-1}$, H_2/CO_2 = 4, 6.1 bar.

Figure S6. SEM micrographs for the reduced: $10\%Ni/TiO_2$ and $10\%Ni\text{-}S/TiO_2$ catalysts.

Figure S7. Particle size distributions (Ni species only) based on total Ni particle number and on total Ni atom number for the fresh and reduced: **a** $10\%Ni/TiO_2$ and **b** $10\%Ni\text{-}S/TiO_2$ catalysts.

Figure S8. EDX analyses for the fresh and reduced: **a** $10\%Ni/TiO_2$ and **b** $10\%Ni\text{-}S/TiO_2$ catalysts.

Figure S9. XRD diagrams for the $TiOSO_4.xH_2O$ reference compound before (black line) and after reaction in the presence of a 1/4 mixture of N_2/H_2 at atmospheric pressure, at 400 °C for 4 h (red line).

Figure S10. XRD diagrams for the reduced: **a** $10\%Ni/TiO_2$ and **b** $10\%Ni\text{-}S/TiO_2$ catalysts.

Figure S11. High-resolution Ni 2p, S 2p and Ti 2p spectra of the $10\%Ni/TiO_2$ and $10\%Ni\text{-}S/TiO_2$ catalysts.

Figure S12. High-resolution Ti 2p spectra of TiO_2, and $TiOSO_4.xH_2O$ reference compounds, and $10\%Ni\text{-}S/TiO_2$ catalyst.

Figure S13. Raman spectra of TiO_2-P25, $TiOSO_4.xH_2O$, the $10\%Ni/TiO_2$ catalyst and the $10\%Ni\text{-}S/TiO_2$ catalyst (532 nm excitation).

Figure S14. EPR spectrum of the $10\%Ni\text{-}S/TiO_2$ catalyst.

Figure S15. TPR profiles of the 10%Ni/TiO_2 and 10%Ni-S/TiO_2 catalysts.

Figure S16. CO binding modes to various facets of the Ni_xS_y systems.

Table S2. Binding energy of CO to various facets of the Ni_xS_y systems The relative energies are difference in energies relative to the most stable structure.

Figure S17. Charge density isosurfaces for all surfaces studied. The regions of highest negative potential for binding are depicted in green. In summary, dangling anions are likely locations for S-C binding, but CO_2 may also be activated by Ni-O bond formation. Isosurfaces are plotted at 0.01 e/A^3 and colored using the electrostatic potential.

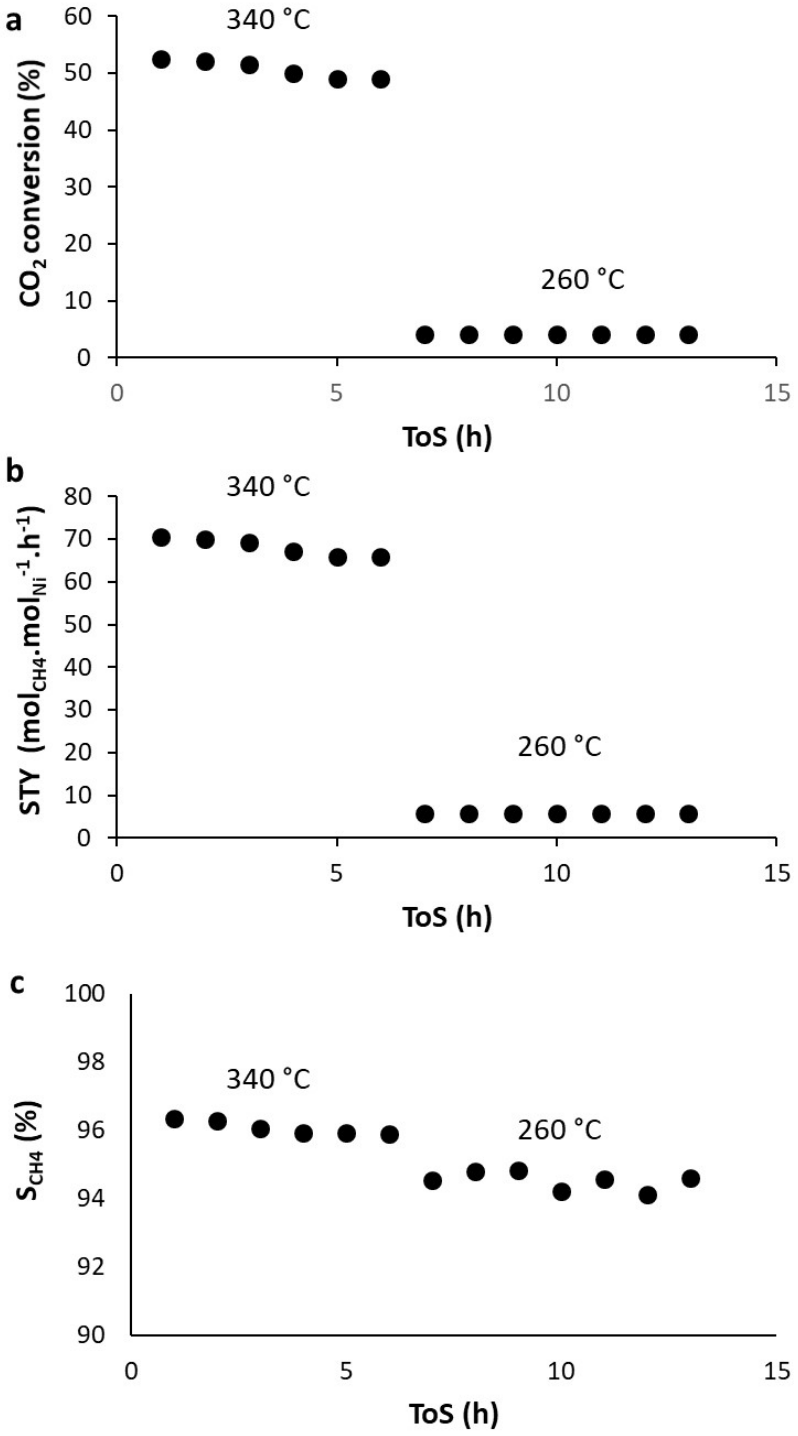

Figure S1. The curves of: **a** CO_2 conversion, **b** STY and **c** selectivity *versus* ToS at different temperatures over the 10Ni/TiO_2 catalyst; reaction conditions: 200 mg catalyst, *F/W* = 33 000 mL.g^{-1}.h^{-1}, H_2/CO_2 = 4, 6.1 bar.

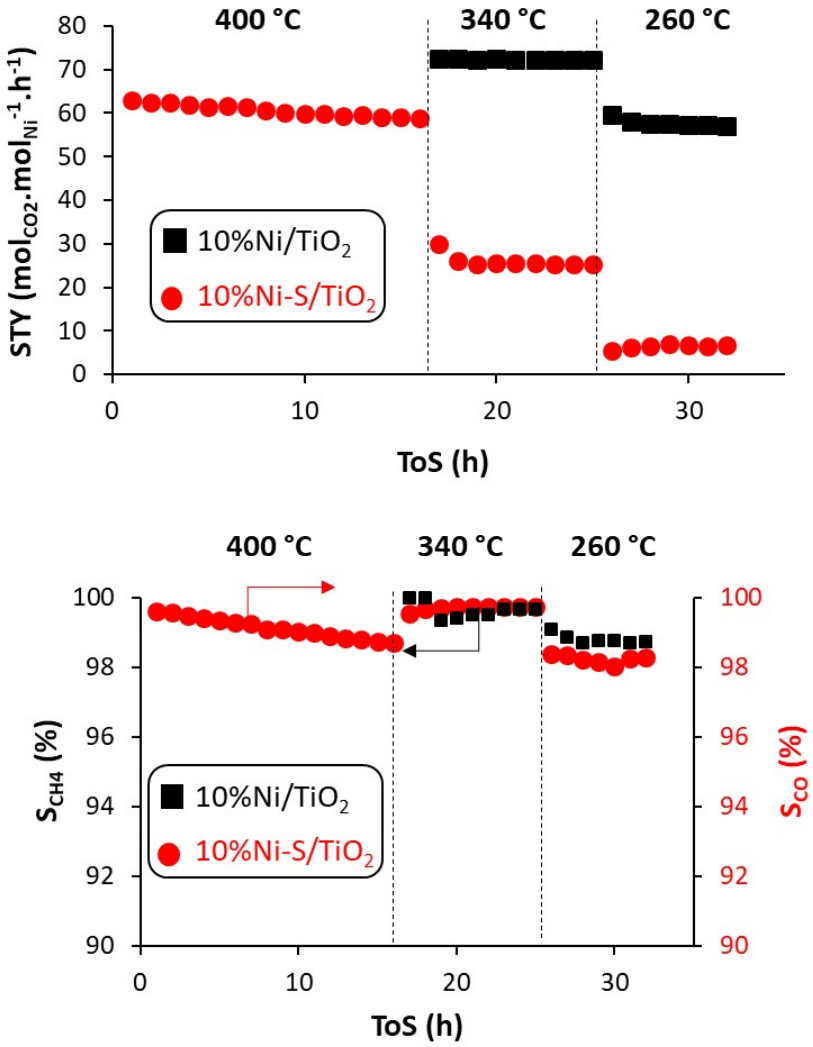

Figure S2. The curves of the CO_2 conversion rate and selectivity *versus* ToS at different temperatures over the 10Ni/TiO_2 (black squares) and 10Ni-S/TiO_2 (red circles) catalysts; reaction conditions: 200 mg catalyst, *F/W* = 16 500 mL.g^{-1}.h^{-1}, H_2/CO_2 = 4, 6.1 bar.

Table S1. Catalytic performances of supported Ni-based catalysts for the RWGSR.

Catalyst	Ni (%)	T (°C)	P (bar)	CO_2/H_2 (vol)	F/W ($mL.g^{-1}.h^{-1}$)	CO_2 conv. (%)	STY_{CO2} ($mol_{CO2}.mol_{Ni}^{-1}.h^{-1}$)	Product rate ($mol_{CO2}.g_{cat.}^{-1}.h^{-1}$)	S_{CO} (%)	Ref.
Ni/Mg(Al)O	1.1	700	1	1/3	540 000	56	96	0.018	94	[1]
Ni/SiO_2	2.4	660	1	1/4	400 000	64	549	0.224	100	[2]
Ni/MgO	7	600	1	1/1	15 000	34	88.9	0.106	93	[3]
Ni/SBA-15	1	500	1	1/1	1 200 000	12	1880	0.320	96.7	[4]
$LaCo_{0.9}Ni_{0.1}O_3$	2.8	475	1	1/1	48 000	30.8	347	0.165	98.8	[5]
$LaFe_{0.5}Ni_{0.5}O_3$	12	400	1	1/2	24 000	16.3	9	0.023	96.6	[6]
Ni_3Fe_3/ZrO_2	1.51	400	1	1/2	24 000	18.6	89.7	0.002	95.8	[7]
Ni/SiO_2	15	400	1	1/4	400 000	36	50.2	0.128	>99	[8]
$Mg_{0.9}Ni_{0.1-x}Al_2O_4$	4.2	400	1	1/4	36 000	6.5	349	0.250	96.2	[9]
$Ni-S/TiO_2$	7.6	400	6.1	1/4	16 000	76.2	60.6	0.080	99.1	*This work*
$Ni-S/TiO_2$	7.6	340	6.1	1/4	33 000	51.1	68.1	0.088	96	*This work*

[1] M. T. Rodrigues, P. C. Zonetti, O. C. Alves, E. F. Sousa-Aguiar, L. E. P.Borges, L. G. Appel, , *Applied Catalysis A: General*, 2017, **543**, 98-103.

[2] R. V. Gonçalves, L. L. R.Vono, R. Wojcieszak, C. S. B.Dias, H. Wender, E.Teixeira-Neto, L. M.Rossi, *Applied Catalysis B: Environmental*, 2017, **209**, 240-246.

[3] A. Ranjbara, A. Irankhahb,. S. F. Aghamiri, J. Environmental Chemical Engineering 2018, **6**, 4945–4952.

[4] H. Liu, L. Wang, Crystals, 2021, **11**, 790.

[5] H. S. Lim, M. Lee, Y. Kim, D. Kang and J. W. Lee, *International Journal of Hydrogen Energy*, 2021, **46**, 15497-15506.

[6]. B. Zhao, B. Yan, Z. Jiang, S. Yao, Z. Liu, Q.Wu, R. Ran, S. D. Senanayake, D. Weng, J. G. Chen, *Chemical Communications*, 2018, **54**, 7354-7357.

[7] B. Yan, B. Zhao, S. Kattel, Q. Wu, S. Yao, D. Su and J. G. Chen, *Journal of Catalysis*, 2019, **374**, 60-71.

[8] T. S. Galhardo, A. H. Braga, B. H. Arpini, J. Szanyi, R. V. Gonçalves, B. F. Zornio, C. R. Miranda and L. M. Rossi, *Journal of the American Chemical Society*, 2021, **143**, 4268-4280.

[9] K. Feng, J. Tian, M. Guo, Y. Wang, S. Wang, Z. Wu, J. Zhang, L. He and B. Yan, *Applied Catalysis B: Environmental*, 2021, **292**, 120191.

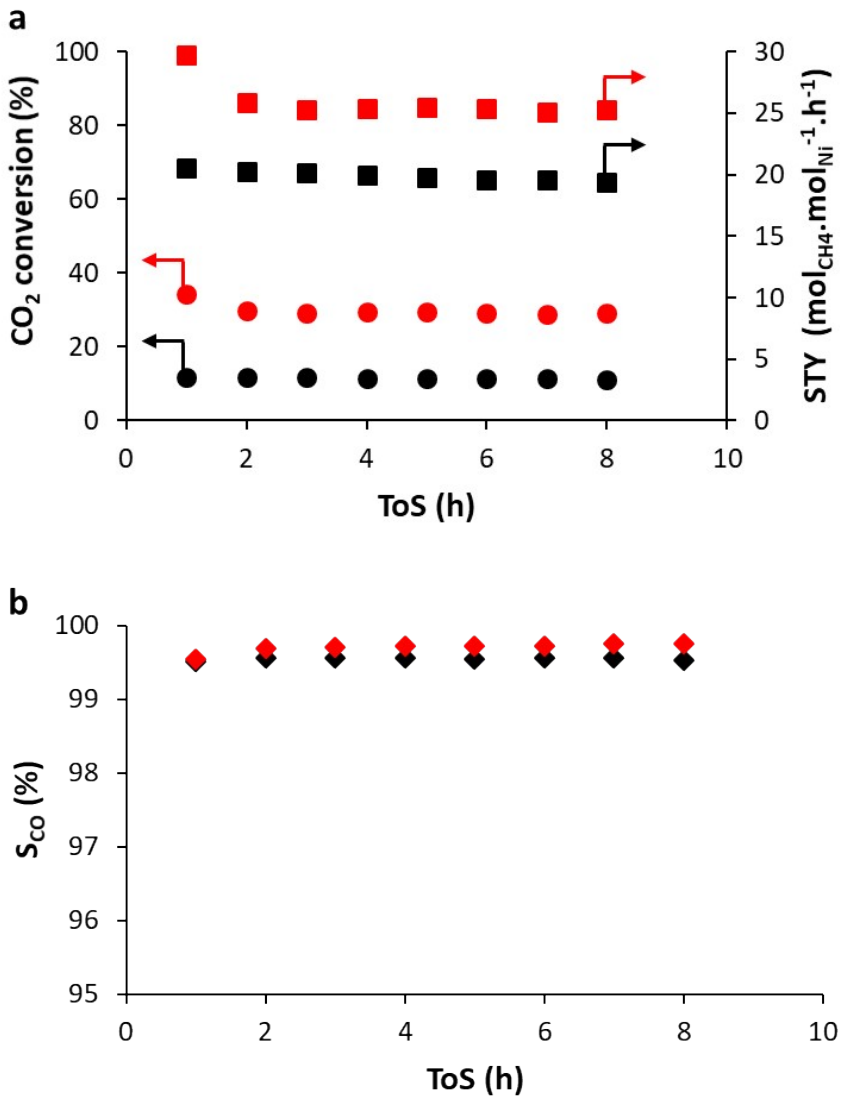

Figure S3. The curves of the CO_2 conversion, conversion rate and selectivity *versus* ToS at different *F/W* ratio over the 10Ni-S/TiO_2 catalysts. **a** CO_2 conversion at *F/W* = 16 500 mL.g^{-1}.h^{-1} (red circles) and *F/W* = 33 000 mL.g^{-1}.h^{-1} (black circles); and CO_2 conversion rate at *F/W* = 16 500 mL.g^{-1}.h^{-1} (red squares) and *F/W* = 33 000 mL.g^{-1}.h^{-1} (black squares). **b** Selectivity towards CO at *F/W* = 16 500 mL.g^{-1}.h^{-1} (red diamonds) and *F/W* = 33 000 mL.g^{-1}.h^{-1} (black diamonds).

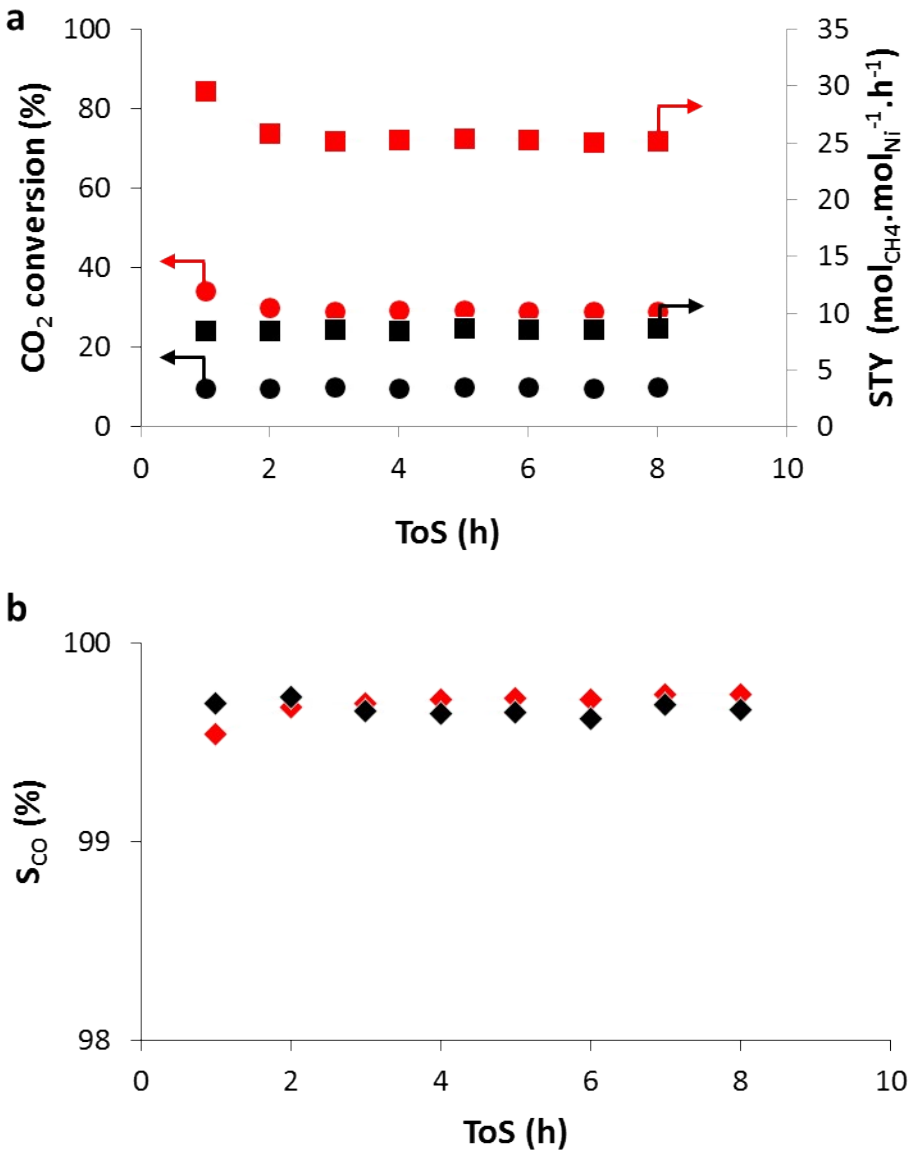

Figure S4. The curves of the CO_2 conversion, conversion rate and selectivity *versus* ToS at different pressure over the 10Ni-S/TiO_2 catalysts. **a** CO_2 conversion at 6.1 bar (red circles) and 1 bar (black circles); and CO_2 conversion rate at 6.1 bar (red squares) and 1 bar (black squares). **b** Selectivity towards CO at 6.1 bar (red diamonds) and 1 bar (black diamonds). T = 340 °C.

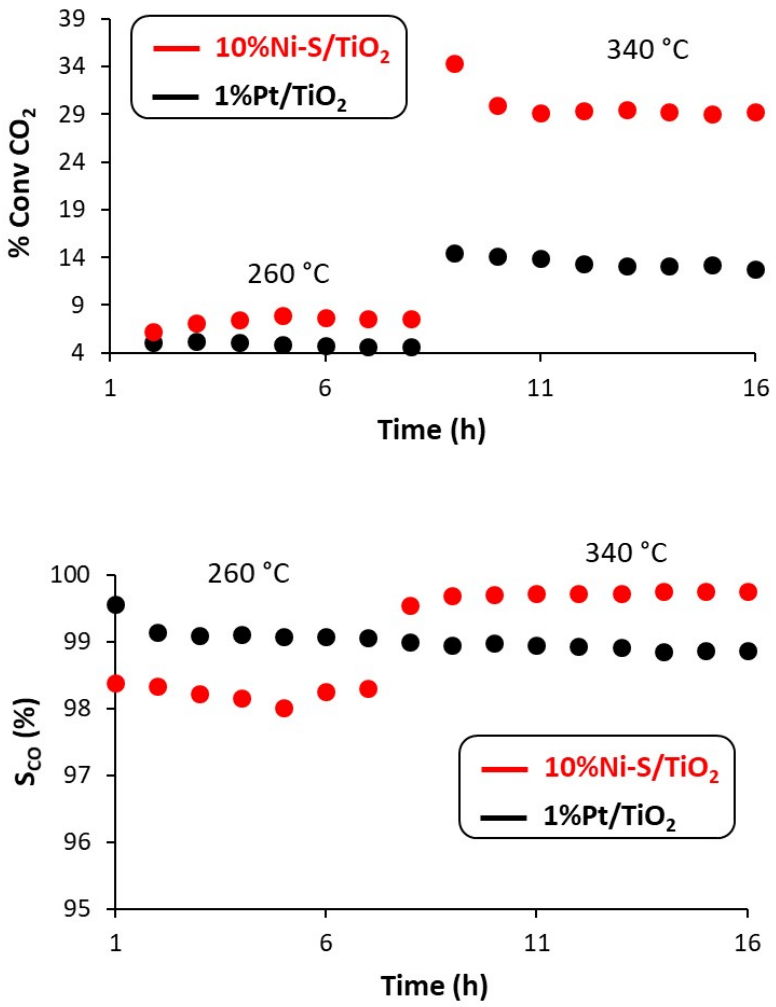

Figure S5. The curves of the CO_2 conversion and CO selectivity *versus* ToS at different temperatures over the $1Pt/TiO_2$ (black circles) and $10Ni\text{-}S/TiO_2$ (red circles) catalysts; reaction conditions: 200 mg catalyst, *F/W* = 16 500 $mL.g^{-1}.h^{-1}$, H_2/CO_2 = 4, 6.1 bar.

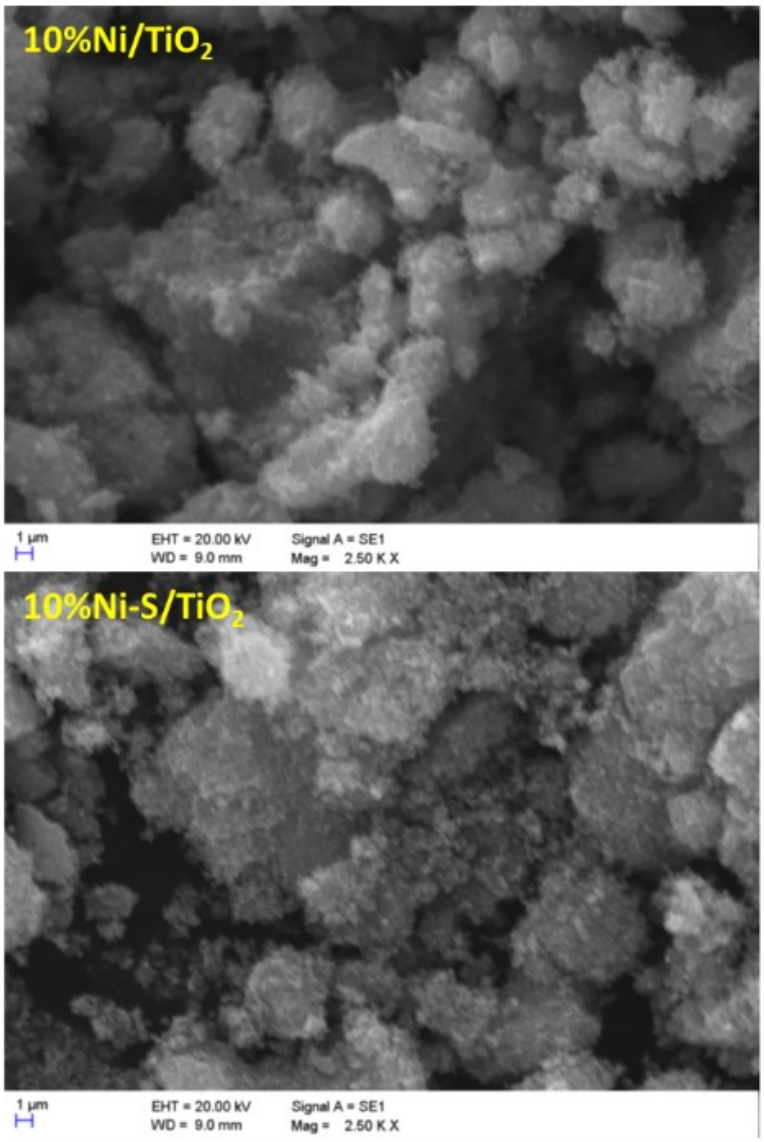

Figure S6. SEM micrographs for the reduced: 10%Ni/TiO_2 and 10%Ni-S/TiO_2 catalysts.

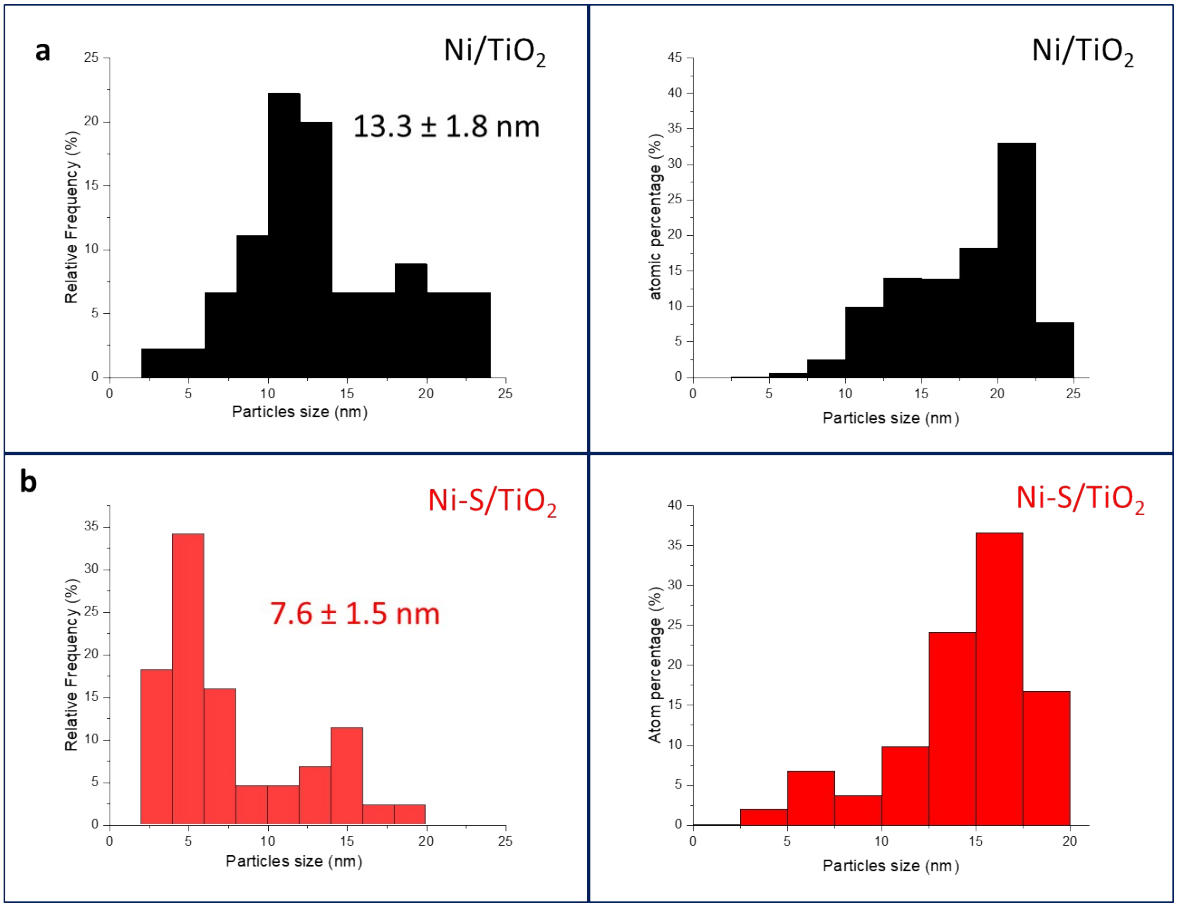

Figure S7. Particle size distributions (Ni species only) based on total Ni particle number and on total Ni atom number for the fresh and reduced: **a** 10%Ni/TiO_2 and **b** 10%Ni-S/TiO_2 catalysts.

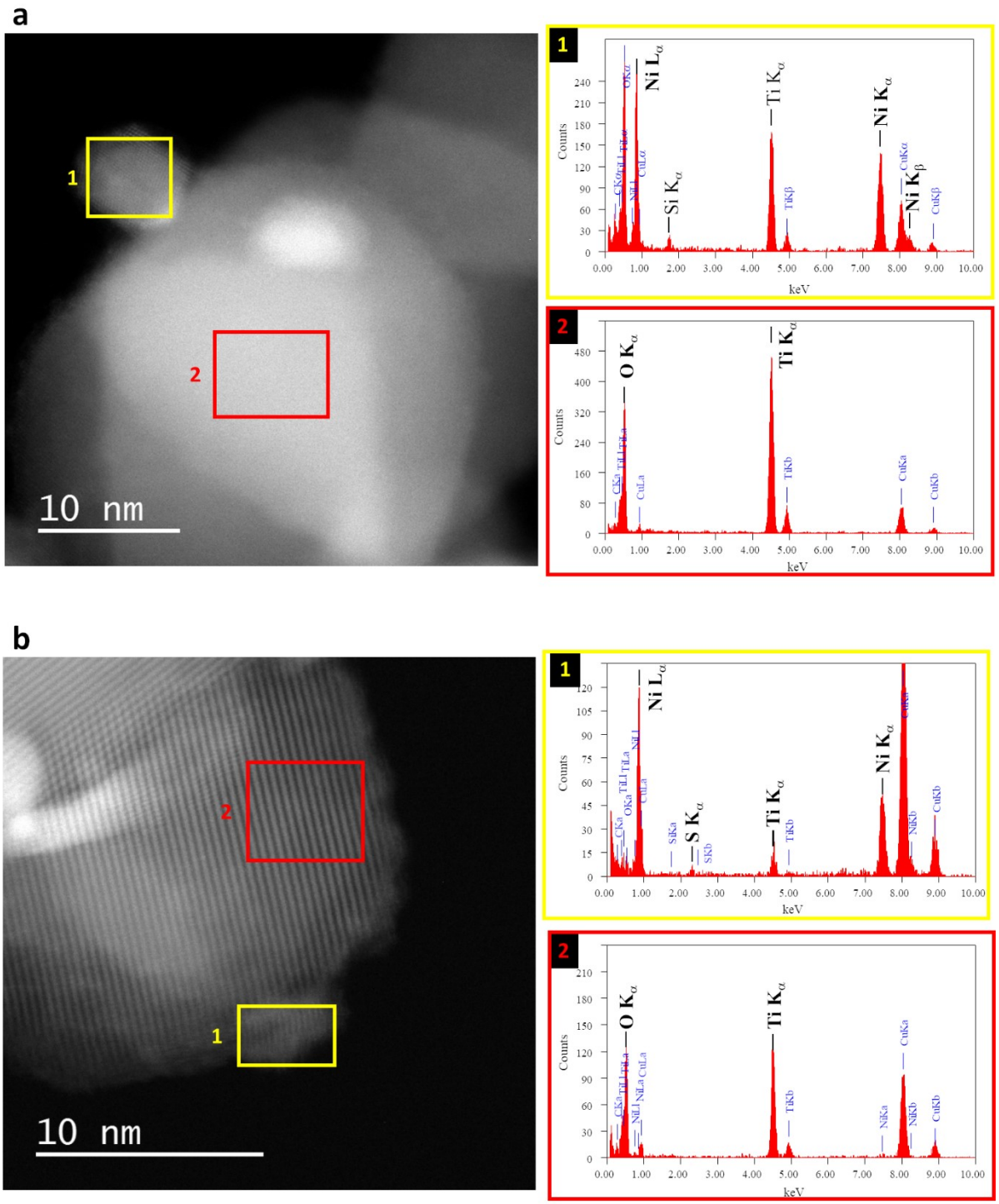

Figure S8. EDX analyses for the fresh and reduced: **a** 10%Ni/TiO_2 and **b** 10%Ni-S/TiO_2 catalysts.

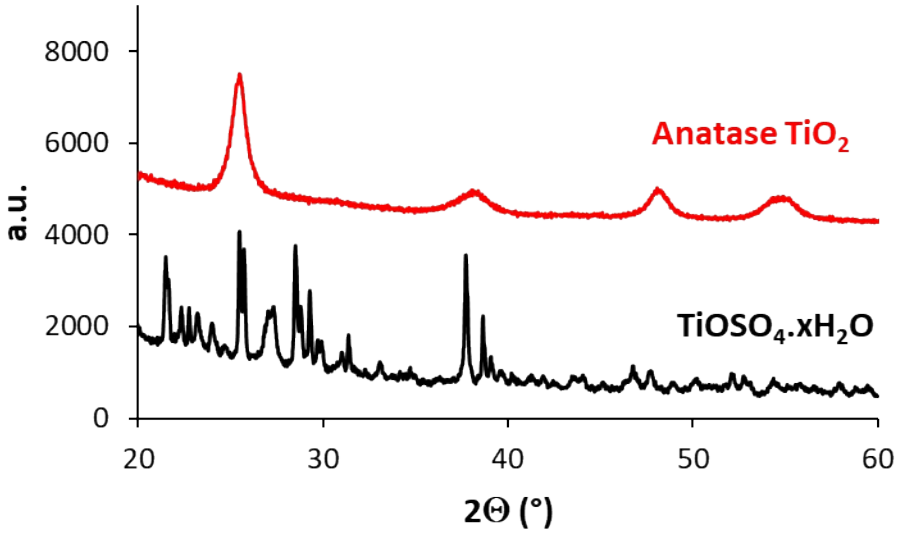

Figure S9. XRD diagrams for the $TiOSO_4.xH_2O$ reference compound before (black line) and after reaction in the presence of a 1/4 mixture of N_2/H_2 at atmospheric pressure, at 400 °C for 4 h (red line).

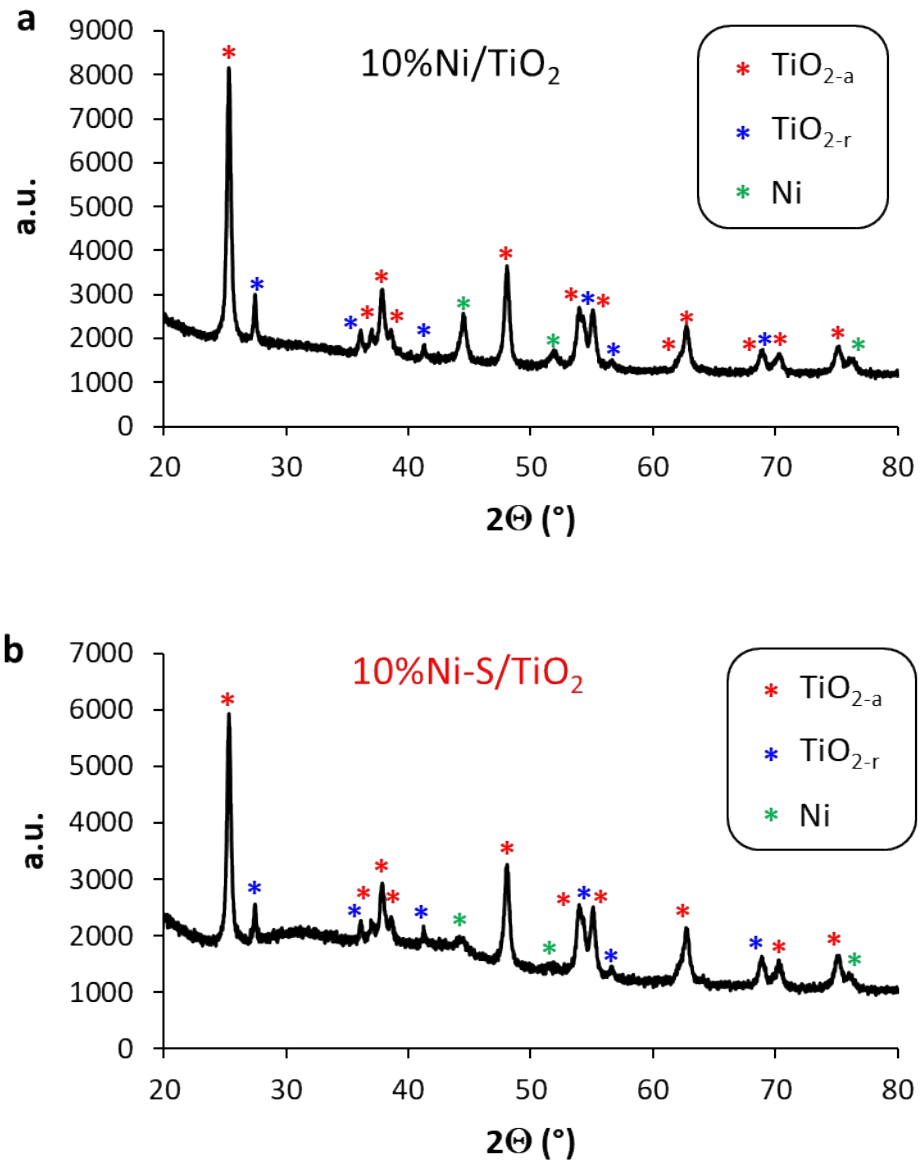

Figure S10. XRD diagrams for the reduced: **a** 10%Ni/TiO_2 and **b** 10%Ni-S/TiO_2 catalysts.

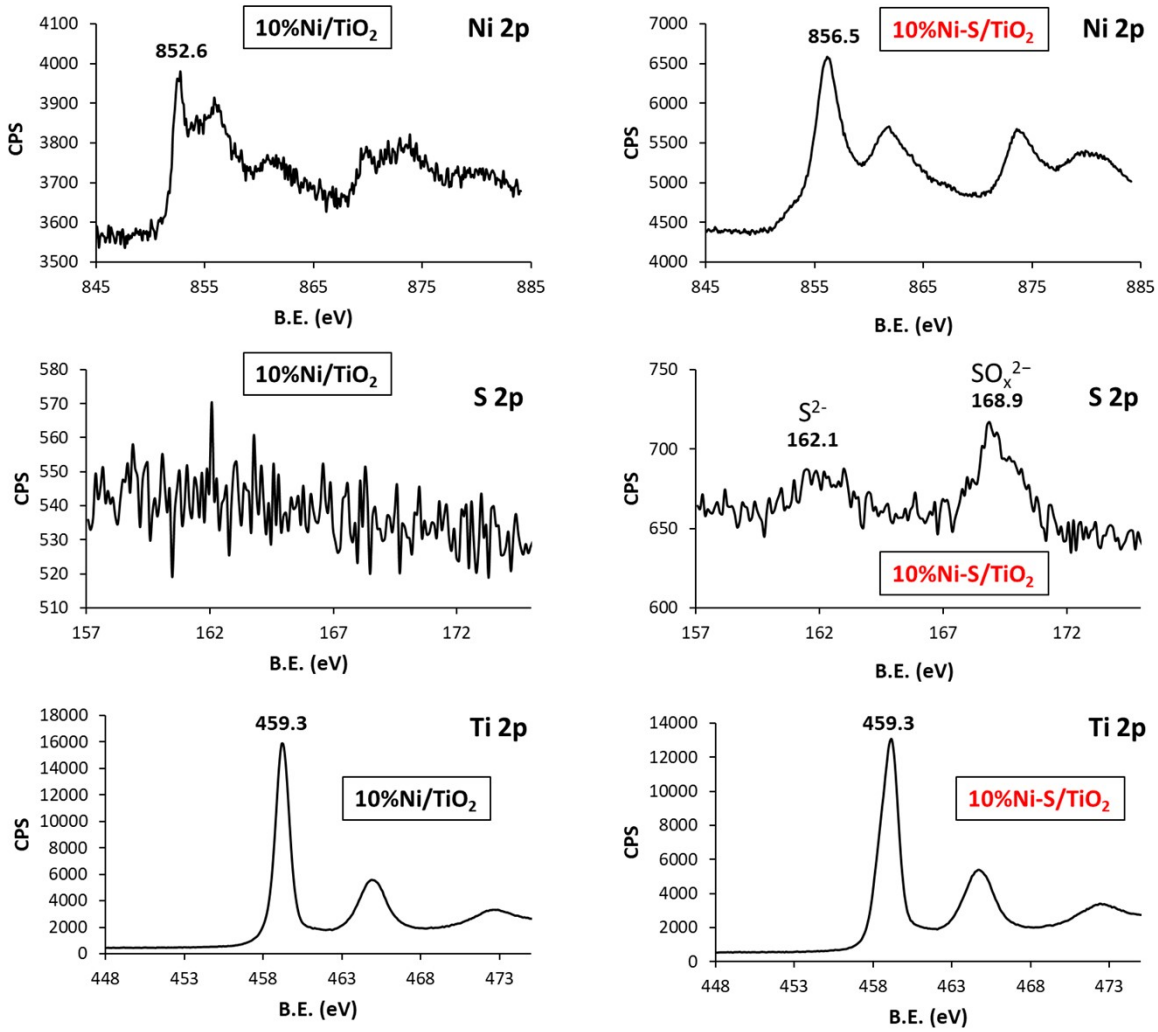

Figure S11. High-resolution Ni 2p, S 2p and Ti 2p spectra of the 10%Ni/TiO_2 and 10%Ni-S/TiO_2 catalysts.

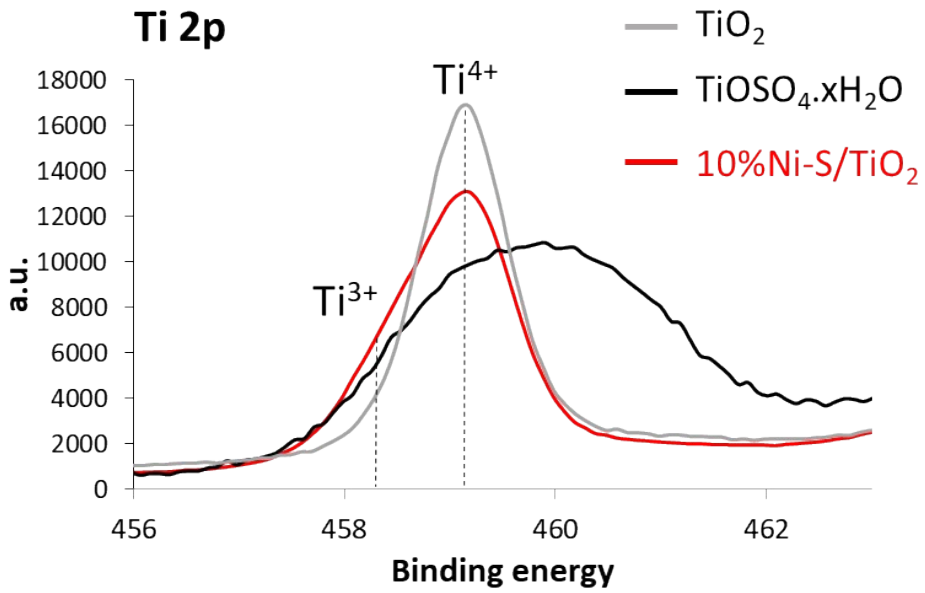

Figure S12. High-resolution Ti 2p spectra of TiO_2, and $TiOSO_4.xH_2O$ reference compounds, and 10%Ni-S/TiO_2 catalyst.

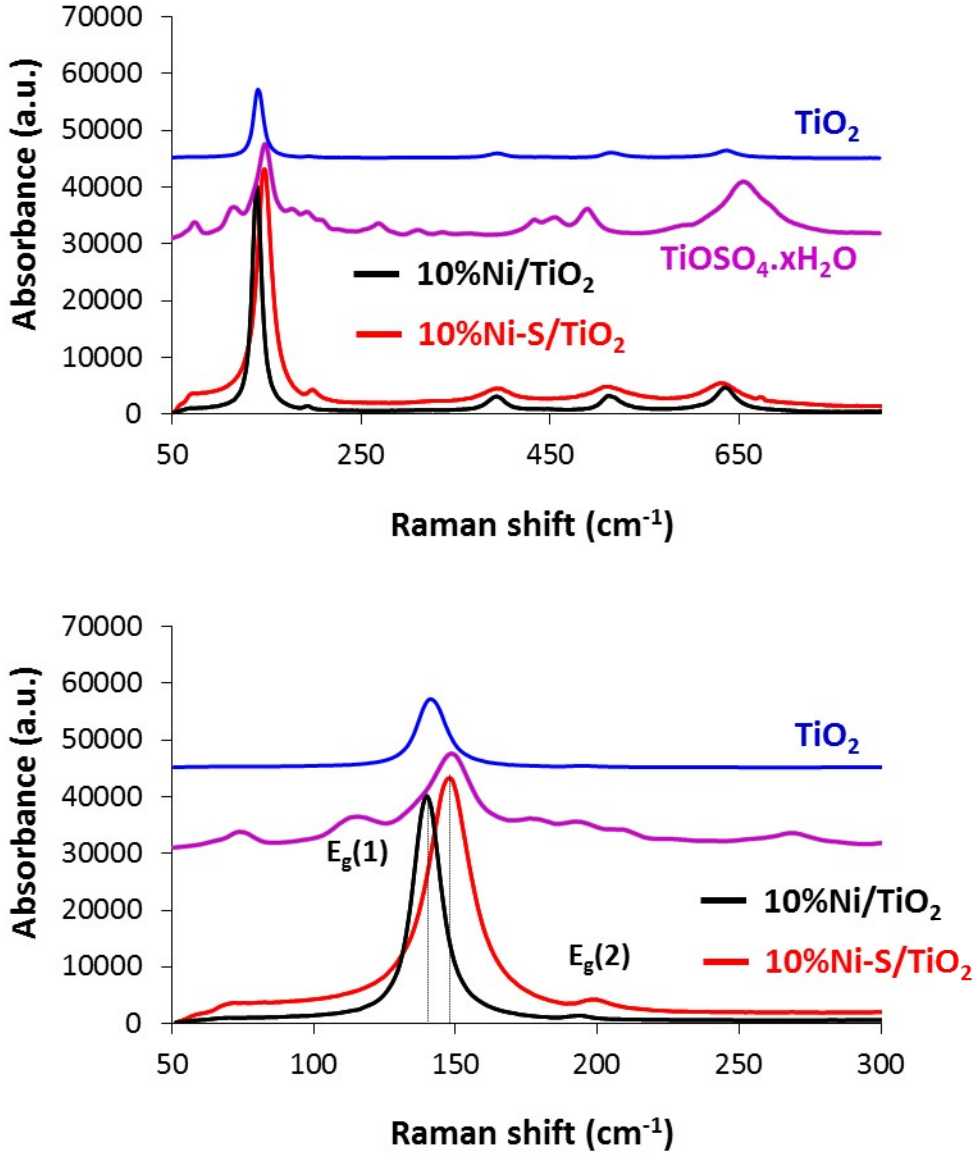

Figure S13. Raman spectra of TiO_2-P25, $TiOSO_4.xH_2O$, the 10%Ni/TiO_2 catalyst and the 10%Ni-S/TiO_2 catalyst (532 nm excitation).

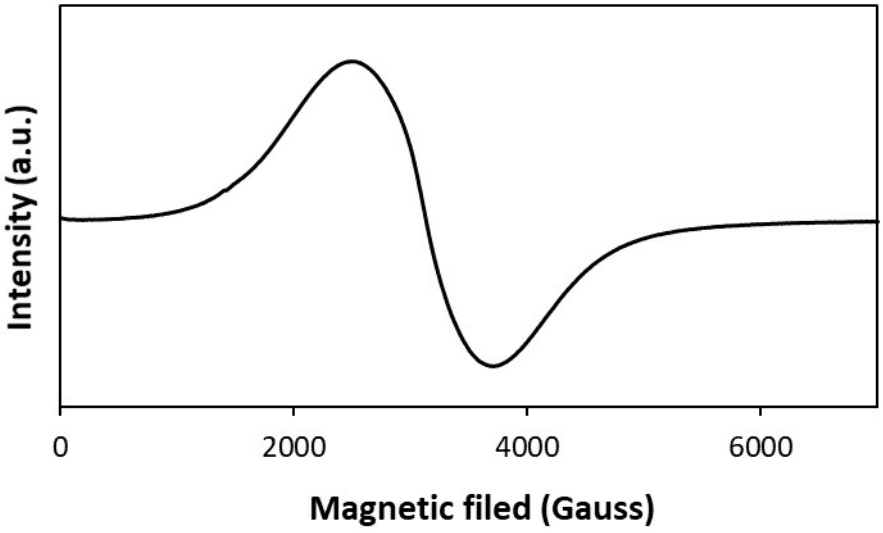

Figure S14. EPR spectrum of the 10%Ni-S/TiO_2 catalyst.

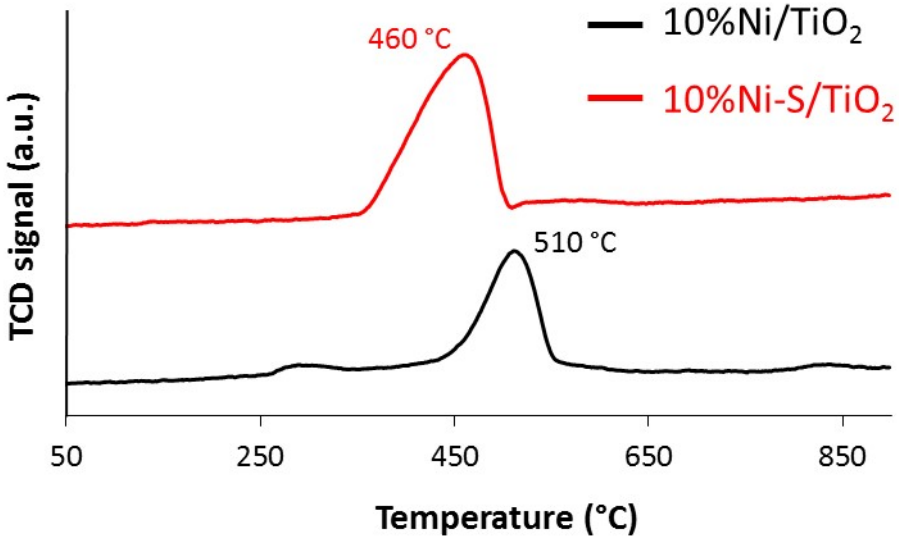

Figure S15. TPR profiles of the 10%Ni/TiO_2 and 10%Ni-S/TiO_2 catalysts.

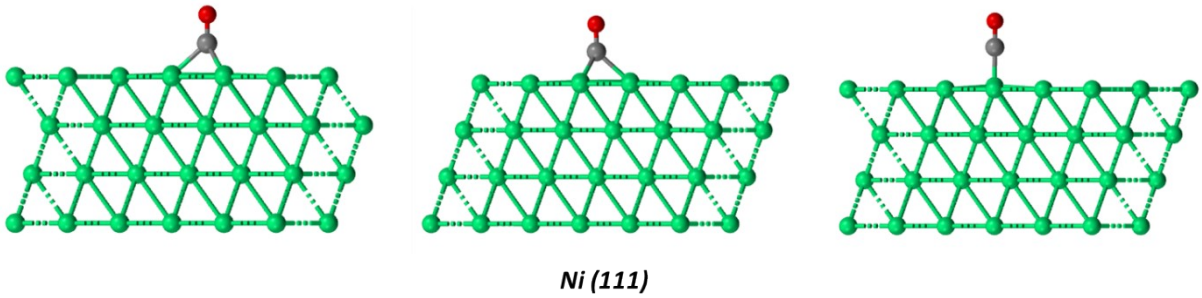

Ni (111)

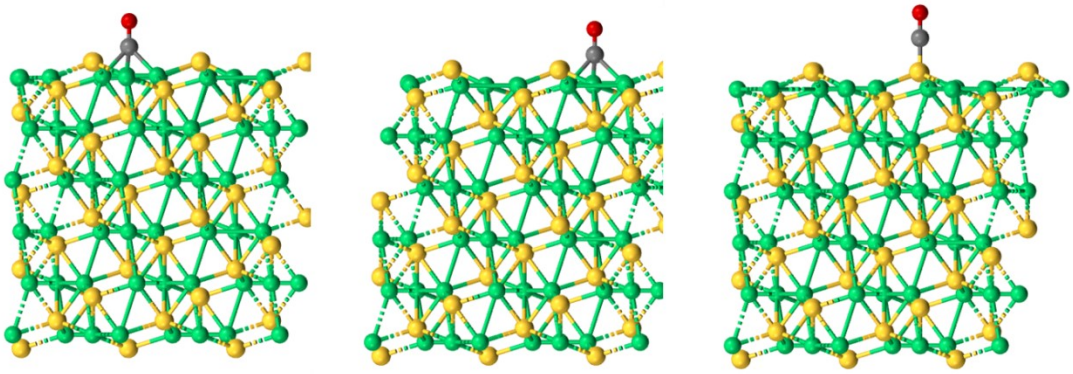

Ni_3S_2 (111)

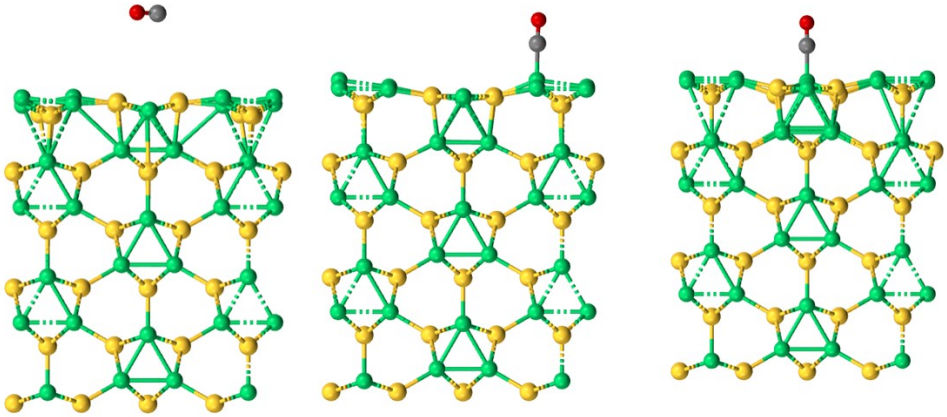

NiS (100)

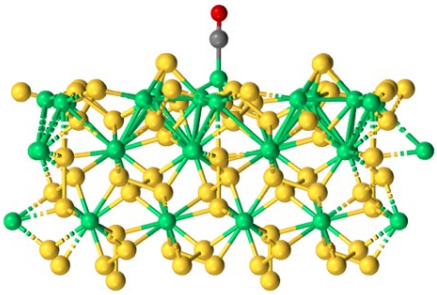

NiS_2 (111)

Figure S16. CO binding modes to various facets of the Ni_xS_y systems.

Table S2. Binding energy of CO to various facets of the Ni_xS_y systems The relative energies are difference in energies relative to the most stable structure.

Configuration	Relative Energy (eV)*	Adsorption energy (eV)
Ni111_CO_min	0.00	-1.57
Ni111_CO_alternate1	0.00	-1.57
Ni111_CO_alternate2	0.00	-1.57
Ni111_CO_alternate3	0.28	-1.29
NiS100_CO_min.cif	0.00	-1.20
NiS100_CO_alternate1	0.07	-1.13
NiS100_CO_alternate2	1.04	-0.16
NiS100_CO_alternate3	1.23	0.03
$NiS_2$111_CO_min		-0.73
$Ni_3S_2$001_CO_min	0.00	-1.47
$Ni_3S_2$001_CO_alternate1	0.01	-1.46
$Ni_3S_2$001_CO_alternate2	0.02	-1.44
$Ni_3S_2$001_CO_alternate3	2.07	0.60

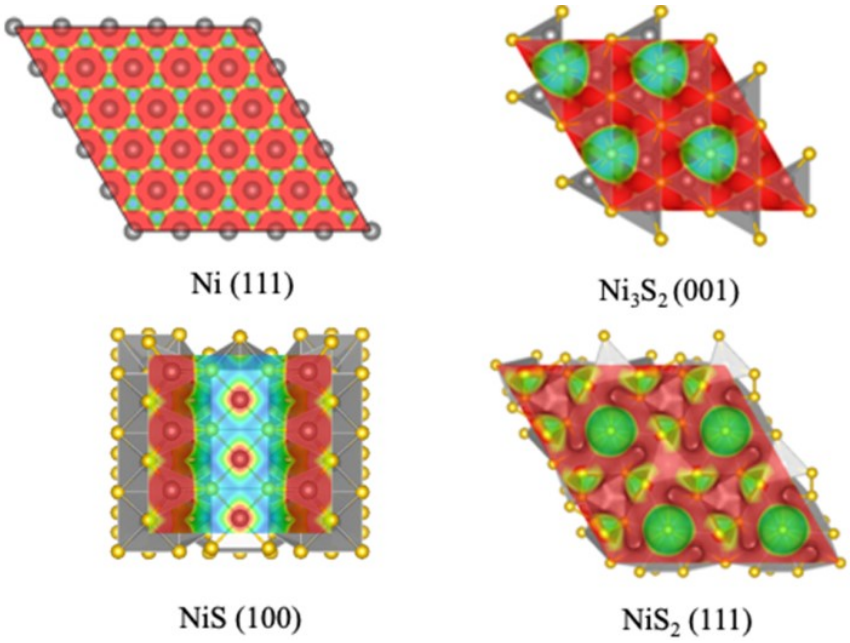

Figure S17. Charge density isosurfaces for all surfaces studied. The regions of highest negative potential for binding are depicted in green. In summary, dangling anions are likely locations for S-C binding, but CO_2 may also be activated by Ni-O bond formation. Isosurfaces are plotted at 0.01 e/A^3 and colored using the electrostatic potential.